# Target detection with a low-power holographic detector

**Sri Rama Prasanna Pavani and Lingfei Meng**
*Ricoh Innovations Inc., 2882 Sand Hill Road Suite 115, Menlo Park, CA 94025-7057, USA*
*prasanna@rii.ricoh.com*

**Abstract:** We demonstrate broadband and wide-field detection of targets such as logos and QR codes with a low-power target-detector that uses a hologram encoding target-features for incoherent optical correlation and two single-pixel detectors for high-speed detection.
**OCIS codes:** (100.4999) Pattern recognition, target tracking; (070.4550) Correlators; (110.1758) Computational Imaging

## 1. Introduction

Detection of objects that exhibit a known set of spatial features is valuable in surveillance, factory automation, automotive, consumer electronics, and retail applications. Standard computer-vision based target detection approaches consume well over 100mW for image acquisition and processing [1,2]. Placing this number in context, 100mW is over 10x higher power that what a modern smart phone, for instance Samsung Galaxy SIII, consumes in its standby mode. Traditional detection methods are therefore unsuitable for power-intense operations such as target monitoring in devices that have a finite battery capacity.

Recently, we had introduced a low-power target detector, called HoloCam, to eliminate the need for image sensor arrays and image processing by encoding target features in a computer generated target hologram (TH) and detecting with a single-pixel distribution sensitive detector and a single-pixel ambient light detector [3]. In this paper, we report on an improved HoloCam that has better imaging properties to detect targets with 1) wide field of view with reduced off-axis aberrations and 2) improved light efficiency to operate under white LED light scattered by targets. We then discuss our detection methodology using Bayes decision theory and demonstrate detection of QR codes and logos with our improved system.

## 2. HoloCam: Low-power target detector

HoloCam detects targets by optically correlating incoherent broadband light scattered by an object with the impulse response of a TH. The correlation response contains peaks when a target is detected. In contrast, the response reduces to a blur when a non-target is detected. A large-area single-pixel distribution sensitive detector (DSD) generates a high electrical output for the blurry non-target response and a low electrical output for the peaky target response. In addition, an ambient light detector (ALD) is used for normalizing for the overall light scattered by the object, which would otherwise influence the DSD output. The target is detected by calculating a classification metric using current DSD and ALD values, and comparing the metric against a training set of previously known metric values for targets and non-targets.

## 3. Wide-field Detection under scattered Light

Our previous embodiment of HoloCam used a Holoeye PLUTO phase-only spatial light modulator (SLM) for implementing both the target hologram and a Fourier transforming lens. This configuration suffered from two problems: a) poor off-axis imaging performance and b) low correlation response intensity due to high magnification. While the poor off-axis performance is due to the exclusive use of a high-power Fresnel lens (in TH) for focusing, the high magnification results from the smallest achievable focal length being limited by the SLM pixel-pitch.

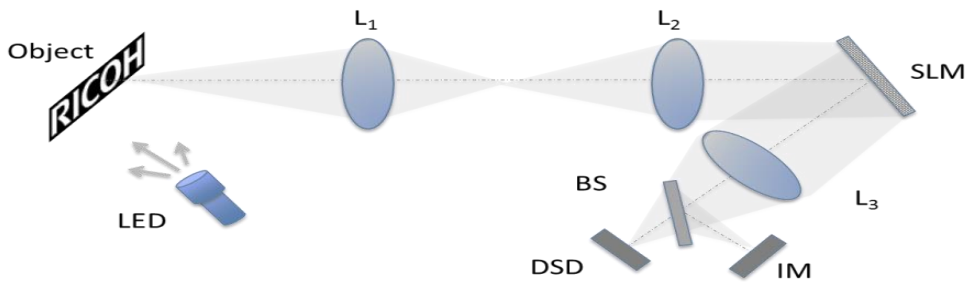


Fig. 1. HoloCam is a low-power wide-field incoherent target detector. $L_1$, $L_2$, and $L_3$ are 25mm, 50mm, and 50mm lenses, respectively. SLM is a spatial light modulator, BS is a beam splitter, IM is an image sensor, and DSD is a distribution sensitive detector.

However, our previous implementation offered the advantage of not focusing unmodulated light originating from suboptimal fill-factor (87%) and polarization-sensitivity of our SLM. This advantage meant that we did not have the need to separate unmodulated light from modulated light using polarizers and gratings (typically encoded in holograms). Gratings, in particular, increase chromatic aberrations and impose a limit on the maximum field of view of our target detector. The field of view limit exists with gratings because the maximum transverse separation of modulated and unmodulated light is limited by the smallest grating-pitch implementable with the SLM.

The system shown in Fig. 1 retains the advantage of not focusing unmodulated light while eliminating the problems of poor off-axis imaging performance and high magnification. In this system, a 25mm Pentax (now, Ricoh) CCTV lens focuses light scattered by the object to the front focal plane of a 4f imaging system whose Fourier plane is modulated by the SLM. A beam-splitter used in the imaging path directs 70% of the captured light towards the DSD and 30% towards a monochrome Aptina image sensor (IM) for response validation. The inclusion of thick lenses in the system provides better off-axis imaging performance. Further, their high focusing power makes it possible to achieve smaller focal lengths and magnification, resulting in high correlation response intensities falling on the DSD. We separate the light modulated by the SLM from the unmodulated light by axially shifting the focal plane of modulated light with a concave lens profile encoded in the TH and locating our detectors in the shifted focal planes. The unmodulated light focuses at the nominal focal plane of the 4f system, and diverges to blur out as a uniform background at the detector planes. Such axial shifting (by adding defocus to the TH) of modulated light is better than transverse shifting (with a grating) for reducing chromatic aberrations and for maximizing the field of view. However, these advantages come at the price of increasing the number of background photons.

A white LED flash light is used to illuminate the object incoherently. In this experimental setup, we did not use an ALD because of controllable illumination conditions. The DSD circuitry consists of a photovoltaic cell whose output is amplified and recorded using a National Instruments USB 6008 data acquisition device.

## 4. Detection Method

The target detection task of HoloCam is treated as a two-class classification problem. The target is denoted as one class $w_1$, and the non-target is denoted as another class $w_2$. The classifier is designed based on Bayes decision theory. Both the target and non-target classes are assumed to follow the Gaussian distribution. The mean and standard deviation of each class is estimated based on training data set. The object is considered as a target if $P(x|w_1)P(w_1) > P(x|w_2)P(w_2)$, where $x$ is the DSD measurement, $P(x|w_i)$ is the conditional probability, and $P(w_i)$ is the probability of class $i$. In our experiment the probabilities of target and non-target are assumed to be equal $[P(w_1) = P(w_2)]$, so the inequality shown above can be simplified as

$$P(x|w_1) > P(x|w_2). \tag{1}$$

The DSD readout (x) is used as an argument to the two-class distributions to calculate the conditional probabilities, and the inequality in eqn. (1) determines the presence or absence of the target.

## 5. QR code and Logo Detection

We now show simulated and experimental results of using HoloCam for detecting QR codes and logos. For QR code detection, we encode features that are common to a set of 83 QR codes (Fig. 2a) in our TH. The common features are predominantly patterns used for position, alignment, and timing in QR codes. We determined these features by averaging the 83 QR codes (Fig. 2b). The average image washes out the data in QR code while highlighting the common features. The average image is used as the target for generating a QR code TH. We design THs by using an iterative optimization method that applies constraints in the TH and DSD planes [3,4,5].

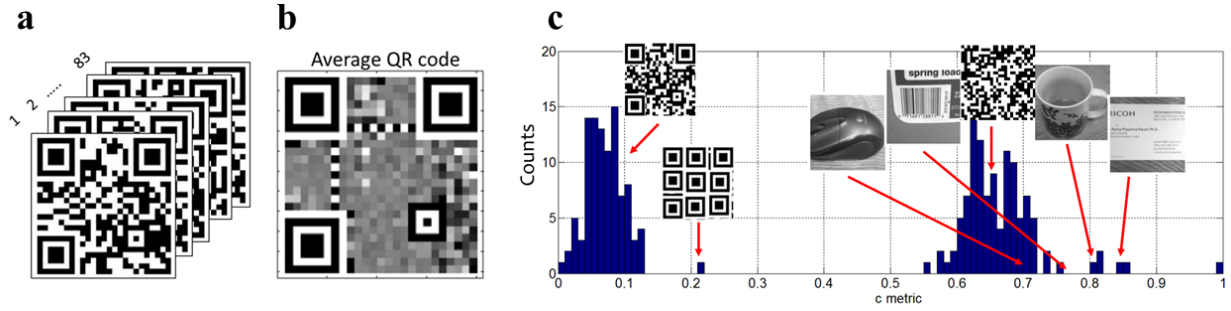


Fig. 2. (a) A set of 83 different QR codes, (b) Average QR code features used for detection, and (c) Detection of QR codes among other common objects. Objects with low c-metric values are detected as QR codes.

Fig. 2c. shows a simulation result of subjecting many commonly found objects to our QR code TH. Each object is cross-correlated with the target encoded in the hologram and a classification metric (c), shown below, is calculated from the resulting correlation response after normalization ($\boldsymbol{I_c}$).

$$c = 1 - k \sum_x \sum_y [\mathbf{1}(x,y) - \boldsymbol{I_c}(x,y)]^2, \tag{2}$$

where $\mathbf{1}(x,y)$ is a uniform matrix of 1s and k is a constant to confine the range of c to [0,1]. The metric c models the response of the DSD by producing low values corresponding to peaky target responses and high values corresponding to blurry non-target responses. Note that all responses $\boldsymbol{I_c}$ are normalized to [0,1] in equation (2). QR code objects encoding different data are seen to take c values between 0 and 0.15 and the other test objects (mouse, random code, mug, etc.) have c values higher than 0.5. A particularly confusing object with position markers similar to QR codes is seen to take a c-value slightly higher than 0.2.

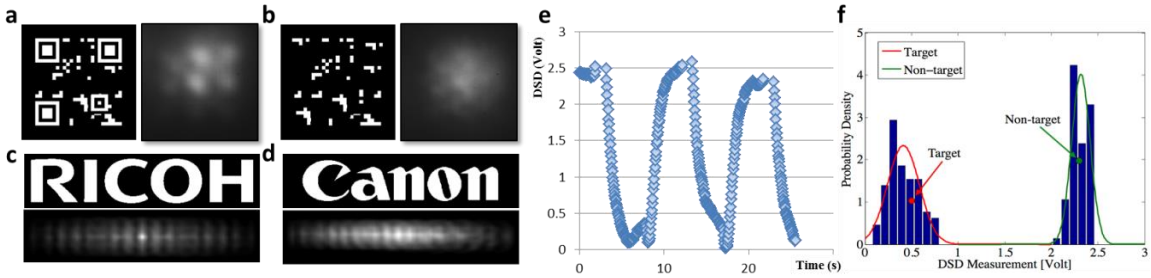


Fig. 3. (a) QR code target and its peaky correlation response, (b) Non target and its blurry response, (c) target logo and its peaky response for logo detection, (d) Non-target logo and its blurry response, (e) DSD output for logo detection. Low voltages correspond to target response, (f) Logo detection using Bayes classifier.

Fig. 3a shows a QR code target (left) and its corresponding experimentally detected correlation response (right) using a TH encoding position and alignment markers. Fig. 3b shows a non-target (without position/alignment markers) and its experimental correlation response to the same TH. Note that the target correlation response exhibits intensity peaks unlike the blurry non-target response.

We now show logo detection results with the HoloCam. Figs. 3c and 3d show simulation results of a system designed to detect RICOH logos [6]. Accordingly, the target hologram is designed to encode the spatial features of the RICOH target. Fig. 3c shows the target and its corresponding correlation response and Fig. 3d shows a non-target and its correlation response. As expected, the target's response exhibits peaks in contrast to the blurry response produced by the non-target. An experimentally detected DSD response for RICOH logo detection is shown in Fig. 3e. In this DSD response, low voltage levels correspond to target correlation response and high voltage levels correspond to non-target response. For repeatability, the target and non-target responses were switched thrice in a ~25 second interval as shown in Fig. 3e. An example of the estimated histogram of DSD measurements for logo detection is shown in Fig. 3f. The histogram shows two distributions with well separated mean DSD levels. The distribution with lower mean is the target (RICOH) distribution and the one with higher mean is the non-target distribution. Gaussian curves are fitted based on the estimated mean and standard deviation. An object is classified as a target or a non-target by using its DSD value to calculate its target and non-target conditional probabilities from the two-class probability distributions.

In the future, we intend to integrate a low-power ALD to the HoloCam system to detect targets under varying illumination conditions.

## 6. Conclusion

We have demonstrated QR code and logo detection with a holographic target detector using broadband incoherent light. The use of holograms and distribution sensitive detectors simplifies and enables low-power target detection.

## 7. References


[1] J. A. Ratches, "Review of current aided/automatic target acquisition technology for military target acquisition tasks," Opt. Eng. 50 (2011).

[2] For instance, OV2720 consumes 111mW in active mode. See http://www.ovt.com/download_document.php?type=sensor&sensorid=91

[3] S. R. P. Pavani et. al, "HoloCam: Low-power wide-field incoherent target detector," OSA COSI, CTu3B.5 (2012).

[4] J. D. Armitage and A. W. Lohmann, "Character Recognition by Incoherent Spatial Filtering," Appl. Opt. 4, 461-467 (1965).

[5] R. Piestun and J. Shamir, "Control of wave-front propagation with diffractive elements," Opt. Lett. 19, 771-773 (1994).

[6] Ricoh is a trademark of Ricoh Company, Ltd. Canon is a registered trademark of Canon, Inc.